Optics Communications 283 (2010) 2719–2723

Contents lists available at ScienceDirect

Optics Communications

journal homepage: www.elsevier.com/locate/optcom

High power nonuniform linear vertical-cavity surface-emitting laser array with a Gaussian far-field distribution

Yan Zhang [a,b], Yongqiang Ning [a,*], Ye Wang [a,b], Jinjiang Cui [c], Guangyu Liu [a,b], Xing Zhang [a,b], Zhenfu Wang [a,b], Te Li [a], Li Qin [a], Yanfang Sun [a], Yun Liu [a], Lijun Wang [a]

[a] Key Laboratory of Excited State Processes, Changchun Institute of Optics, Fine Mechanics, and Physics, Chinese Academy of Sciences, 3888 Southeast Lake Road, Changchun 130033, China
[b] Graduate School of the Chinese Academy of Sciences, Beijing 100049, China
[c] Suzhou Institute of Biomedical Engineering and Technology, China

ARTICLE INFO

Article history:
Received 16 November 2009
Received in revised form 23 February 2010
Accepted 25 February 2010

Keywords:
VCSEL
Array
Far-field angle
High power

ABSTRACT

A 980 nm bottom-emitting vertical-cavity surface-emitting laser (VCSEL) array with a nonuniform linear arrangement is reported to realize high power with a Gaussian far-field distribution. This array is composed of five symmetrically-arranged elements of 200 μm, 150 μm, and 100 μm diameters, with the center spacing of 300 μm and 250 μm respectively. This structure makes it possible to discriminate against the higher order array supermodes. The theoretical simulation of the far-field distribution is in good agreement with the experimental result. An output power of 880 mW with a power density of 1 KW/cm^2 is obtained. The divergence angle is below 20° in the range of operating current from 0 A to 4 A. The comparison between this nonuniform linear array and the conventional two-dimensional array is carried out to demonstrate the good performance of the linear array. A peak power of over 20 W is achieved under a short pulsed operation with a repetition frequency of 1 kHz.

1. Introduction

Dramatic improvements in VCSEL performance have been obtained due to the advances in the fabrication techniques for optical and electrical confinement, as well as in the structural design and growth of Bragg mirrors. [1,2]. VCSELs with an output power of a few mW have been widely used in optical communications, scanning, massive parallel optical interconnections, and so on [3–5]. The applications in solid-state laser pumping, numerous medical applications, high-resolution printing and free-space optical communication are revealing a growing market for high power diode lasers [6–8]. To increase the overall optical output power, the lasing area of the device has to be enlarged. One way is to increase the active area of single devices. However, strong sidelobes appear in the far-field pattern from VCSEL with large aperture, which limits a further increase of the active area. Alternatively, VCSELs are easy to integrate into arrays on a single chip with the merits of simple structure, high array density, high power, and easy heat extraction. But, the conventional two-dimensional (2D) array also has some drawbacks. The increased operation current of the array results in a severe problem in heat dissipation, in return, which might lead to lower power conversion efficiency compared with a single device. Furthermore, the circle or ring beams of individual elements in a 2D array will superimpose and form a periodic intensity distribution with a series of peaks at far field, which means that a part of the output power could not be coupled eventually into fiber. This poor far-field distribution and the necessity of a complex beam shaping system will limit further increasing of the lasing power.

Nonuniform structures of phase-locked diode lasers with variable emitter dimension and spacing can suppress the higher order array supermodes, which results in diffraction limited beams with a single lobe directed perpendicular to the laser facet [9–11]. In this paper, a nonuniform linear VCSEL array is presented. This array is consisted of five VCSELs whose diameters and center spacing decreased, from the central laser to the outermost ones, symmetrically. The purpose of this arrangement is to obtain a compromise among the output power, the power conversion efficiency, and the operation current of the array, and this structure makes it possible to discriminate against the higher order array supermodes, which results in emission with a Gaussian far-field distribution. An output power of 880 mW with a good beam property of Gaussian far-field distribution is demonstrated. In the comparison of the temperature dependent characteristics between this linear array and the conventional 4×4, 2D array is carried out to demonstrate the good performance of the nonuniform linear array. The highest peak power of over 20 W at an injection current of 80 A is achieved under a pulse width of 60 ns and a repetition frequency of 1 kHz.

2. Device structure and process

A schematic cross-section view of a VCSEL structure is displayed in Fig. 1. The VCSEL epitaxy wafers are grown by metal organic chemical

* Corresponding author.
E-mail address: ningyq@ciomp.ac.cn (Y. Ning).

0030-4018/$ – see front matter.
doi:10.1016/j.optcom.2010.02.050

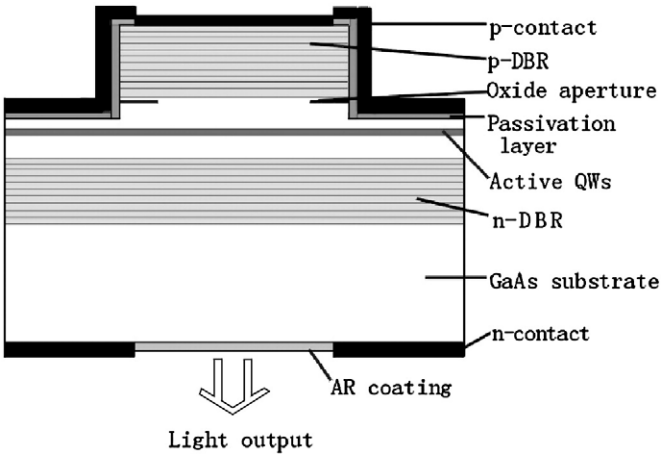

Fig. 1. Schematic diagram of a VCSEL structure.

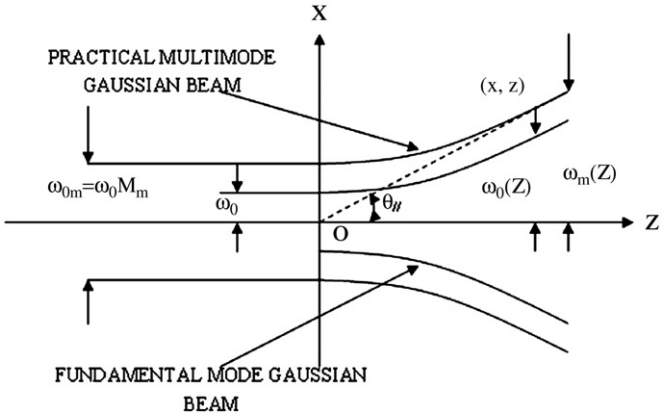

Fig. 3. Relationship between the multimode Gaussian beam and fundamental mode Gaussian beam.

vapor deposition (MOCVD) on n^+-GaAs (100) substrates. Both type DBRs consist of alternating $Al_{0.9}Ga_{0.1}As$ and $Al_{0.1}Ga_{0.9}As$ quarter-wavelength layers with graded interface to reduce series resistance. The active region is composed of three 8 nm thick $In_{0.2}Ga_{0.8}As$ quantum wells (QWs), which are embedded in 10 nm thick GaAs barriers for lasing 980 nm wavelength, and surrounded by AlGaAs claddings to form the one wavelength thick cavity. A single 30 nm thick $Al_{0.98}Ga_{0.02}As$ layer is inserted above a p-type cladding layer in a node of the calculated standing wave pattern, and the layer is oxidized and converted to Al_xO_y in the fabrication process for current confinement.

Wet chemical etching is used to define circular mesa and to expose the layer of $Al_{0.98}Ga_{0.02}As$ for oxidation. The oxidation is carried out in a water vapor atmosphere using nitrogen as the carrier gas at 420 °C to form the current apertures. A SiO_2 passivating layer is deposited on the surface to avoid short circuits when soldering the device on heat sink. After selective etching of the SiO_2 film to form the p-side contact window, TiPtAu is evaporated on the mesa using electron beam deposition. Before depositing an antireflection (AR) coating of HfO_2, the substrate is thinned and polished down to a thickness of 150 μm in order to reduce absorption losses. At the bottom of the GaAs substrate, the light emission window is surrounded by an n-type AuGeNi/Au electrode. The device is cleaved and simply bonded on a copper heat sink with Indium solder, and the junction down bonding method is used due to its efficient heat diffusion.

3. Simulation of far-field distribution

The arrangement of the nonuniform linear array is depicted in Fig. 2, which is composed of five symmetrically-arranged elements with a maximum diameter one of 200 μm at the center, the 150 μm and 100 μm diameter ones at the both sides of the center with the center to center spacing of 300 μm and 250 μm, respectively.

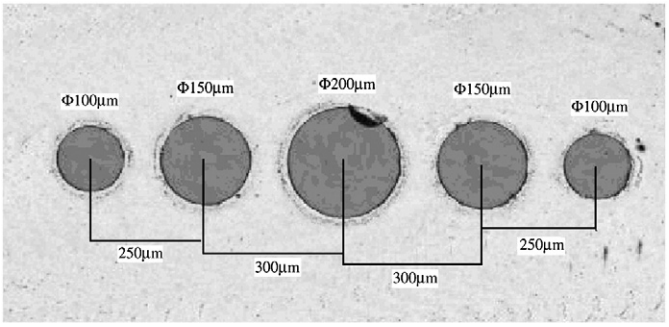

Fig. 2. Schematic diagram of a nonuniform linear array.

The laser beam of each large aperture size element has a multimode Hermite–Gaussian distribution. Assuming the distributions of the modes are independent of each other, the superposition of multimode Hermite–Gaussian distribution is applied on x–z planes. The relationship between a multimode Gaussian beam and a fundamental mode Gaussian beam is shown in Fig. 3, in which $\omega_{0m}=\omega_0 M$ is the width of the multimode Gaussian beam. ω_0 is the width of the fundamental mode Gaussian beam [12]. The distribution of the multimode Gaussian beam intensity can be calculated through the weighted average of $I_i(x,z)$, that is,

$$I_m(x,z) = \sum_{i=0}^{+\infty} C_i I_i(x,z) \tag{1}$$

where C_i is the weight factor,

$$C_i = \frac{2\omega_0^2}{\omega_{0m}^2+\omega_0^2}\left(\frac{\omega_{0m}^2-\omega_0^2}{\omega_{0m}^2+\omega_0^2}\right)^i. \tag{2}$$

Each mode beam intensity distribution is shown as

$$I_i(x,z) = A_i H_i^2\left(\frac{\sqrt{2}}{\omega_0(z)}x\right)\exp\left(-2\frac{x^2}{\omega_0(z)^2}\right). \tag{3}$$

In Eq. (3), $A_i = 2n_{\text{eff}}\sqrt{\frac{\omega\varepsilon_0}{\beta(\pi r_m^2)}}P$, $H_i(x) = (-1)^i e^{x^2}\frac{\partial^i}{\partial x^i}e^{-x^2}$, is the Hermite polynomials.

On inserting Eqs. (2) and (3) into Eq. (1), we obtained

$$I_m(x,z)\propto P\cdot\sum_{i=0}^{+\infty}\frac{2\omega_0^2}{\omega_{0m}^2+\omega_0^2}\left(\frac{\omega_{0m}^2-\omega_0^2}{\omega_{0m}^2+\omega_0^2}\right)^i\cdot H_i^2\left(\frac{\sqrt{2}}{\omega_0(z)}x\right)\exp\left(-2\frac{x^2}{\omega_0(z)^2}\right). \tag{4}$$

With the linear array operated at the current of 4 A, we used the theoretical model [13] to calculate the power value P of each individual element with 100 μm, 150 μm and 200 μm aperture sizes are 0.164 W, 0.367 W, 0.642 W. The corresponding beam quality factors M^2 measured with the lens transform method authenticated by the International Organization for Standardization (ISO) [14] are 35, 47 and 61. The corresponding waists of the elements are 7.66 μm, 8.88 μm, and 10.12 μm by inserting from the waist of the fundamental mode Gaussian beam 1.296 μm [15] into $\omega_{0m}=\omega_0 M$.

After inserting the above parameters of each element into Eq. (4), we could obtain the near-field distribution of the array. A Fourier transform

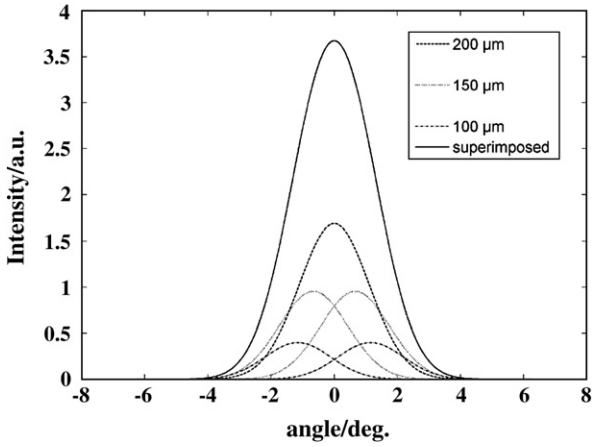

Fig. 4. Superimposed far-field distribution (solid line) of the linear array and far-field distribution of each element (dashed line).

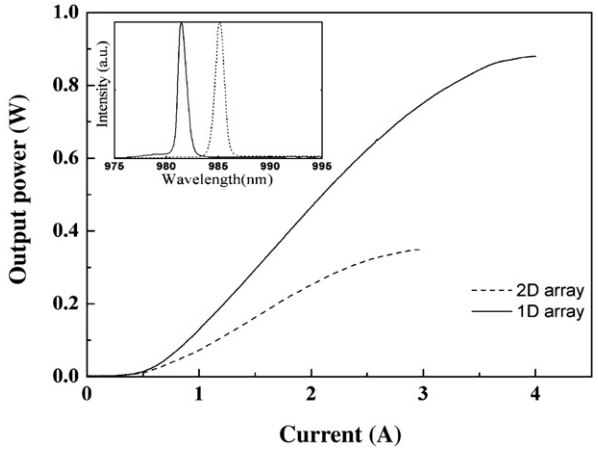

Fig. 6. Dependence of the output power on the current of 1D and 2D arrays. Inset: lasing wavelength at the maximum output power of 1D and 2D arrays.

is made to the near-field Eq. (4) to get the far-field distribution expression, that is,

$$I_m(\theta,z)\propto P\cdot\sum_{i=0}^{+\infty}\frac{2\omega_0^2}{\omega_{0m}^2+\omega_0^2}\left(\frac{\omega_{0m}^2-\omega_0^2}{\omega_{0m}^2+\omega_0^2}\right)^i\cdot H_i^2\left(\frac{\sqrt{2}}{\omega_0(z)}tg(\theta)z\right)\exp\left(-2\frac{tg^2(\theta)z^2}{\omega_0(z)^2}\right) \quad (5)$$

The superimposed far-field distribution at 5 cm away from the lasing aperture is shown in Fig. 4. The solid line represents the superimposed far-field distribution of the linear array, while the other lines correspond to the far-fields of each element.

It is concluded that this structure makes it possible to discriminate against the higher order array supermodes and produce a Gaussian distribution of the beam profile, which is beneficial for the applications of fiber coupling and a high brightness laser source.

4. Experiment results and discussion

The light–current–voltage (L–I–V) of the nonuniform linear array is shown in Fig. 5. The maximum CW optical output power is up to 880 mW at an inject current of 4 A at room temperature and the corresponding optical power density averaged over the total lasing area is 1 KW/cm^2. The threshold current (I_{th}) of the device is about 0.56 A, with the maximum slope efficiency of 0.32 W/A, and the differential resistance (R_d) is 0.09 Ω. The inset of the far-field image in Fig. 5 indicates a Gaussian far-field intensity distribution. As a comparison, the conventional 2D array can only provide a far field with a periodic intensity or a quasi top-hat distribution [16]. The performance of the nonuniform linear array is compared with a 4×4, 2D array with an element aperture of 80 μm and center to center spacing of 130 μm, which has been fabricated from the same VCSEL epitaxy wafer at the same time.

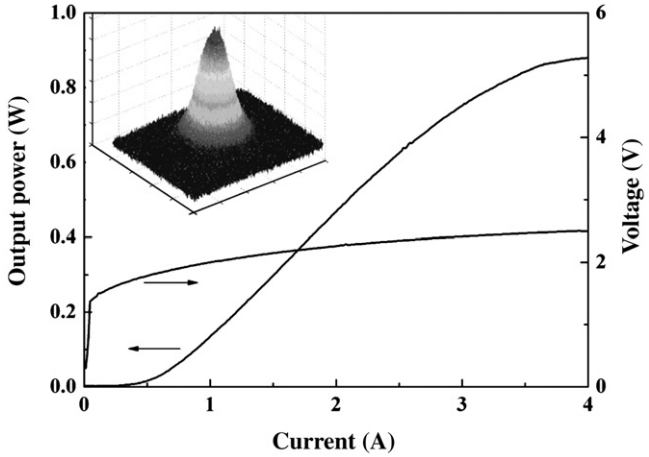

Fig. 5. L–I–V characteristics of a nonuniform linear array.

The dependences of the output power on the current of the two devices are presented in Fig. 6. These two arrays have nearly the same threshold current due to a little difference in the lasing area. Although thermal rollover is observed for all devices, the maximum output power of the linear array (880 mW) is much higher than of a 2D array (350 mW). The reason can be ascribed as follows: the thermal resistance of the 4×4, 2D array with smaller element devices is larger than the linear array. Under CW operation, the larger thermal resistance produces excessive thermal due to the power dissipation, thus increasing the self-heating, causing junction temperature to rise and gain to decrease, and further raising the power dissipation, which in turn further exacerbates the heating, and the cycle continues with the output power decreased until the junction temperature becomes too high to lasing. Furthermore, the high density of the 4×4, 2D array makes the crosstalk of the thermal effect more serious because of the thermal cross resistance inversely proportional to the element spacing [17]. The larger aperture and wider distance of each element in the linear array make it easy for heat extraction, which means it is more suitable for high temperature operation. The lasing wavelengths at the maximum output power of the two devices are shown in the inset of Fig. 6. We can infer that the junction temperature of the linear device is lower from its less redshift of the wavelength.

The far-field lasing intensity distributions of the nonuniform linear array and the 4×4, 2D array are depicted in Fig. 7. For a 2D array, the emissions of individual elements superimpose and form a periodic intenity distribution with a series of peaks at far field as shown in Fig. 7(a). On the contrary, for a linear array with an optimized center to center spacing and diameters of elements, the intensity superimposition of the beams from all elements creates an intensity maximum at the symmetry axis with a divergence as the half-angle at half-maximum intensity of below 20° in the whole range of operating currents from 0 A to 4 A. The inset of Fig. 7(b) is the far-field pattern at a current of 4 A. Due to the circularly symmetric patterns with low beam divergence angle, the beam of the linear array can be easily focused or collimated into a fiber in a simple butt-coupling arrangement for broad applications.

Since VCSEL is not subject to catastrophic optical damage (COD), the VCSEL array does not fail when operated at short pulses at many times with their rollover CW current, making them useful for high power applications. We developed a nanosecond power source delivering a peak current of 80 A with a pulse of 60 ns and 1 kHz repetition

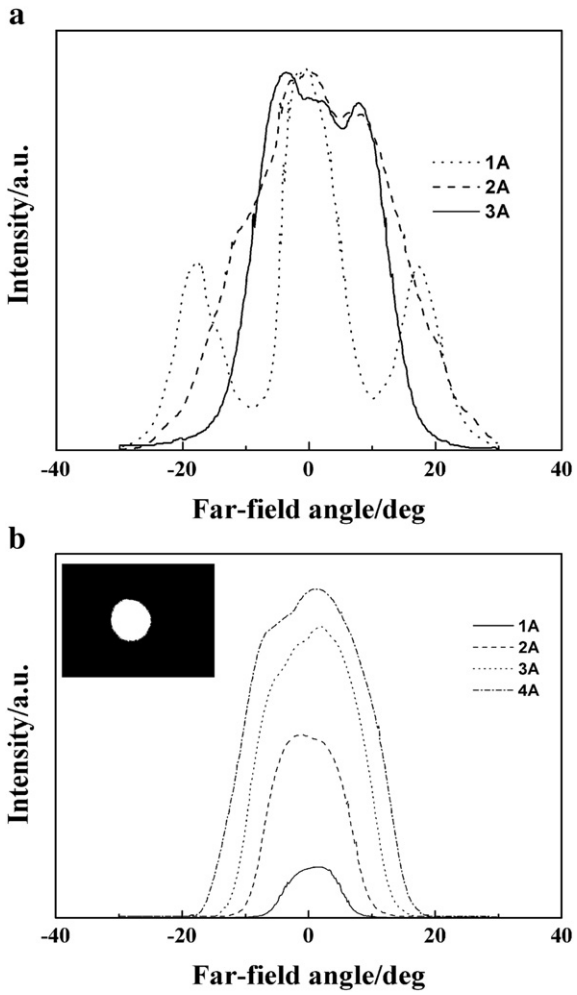

Fig. 7. Far-field lasing intensity distribution. (a) Far-field lasing intensity distribution of 4×4, 2D array. (b) Far-field lasing intensity distribution of linear array.

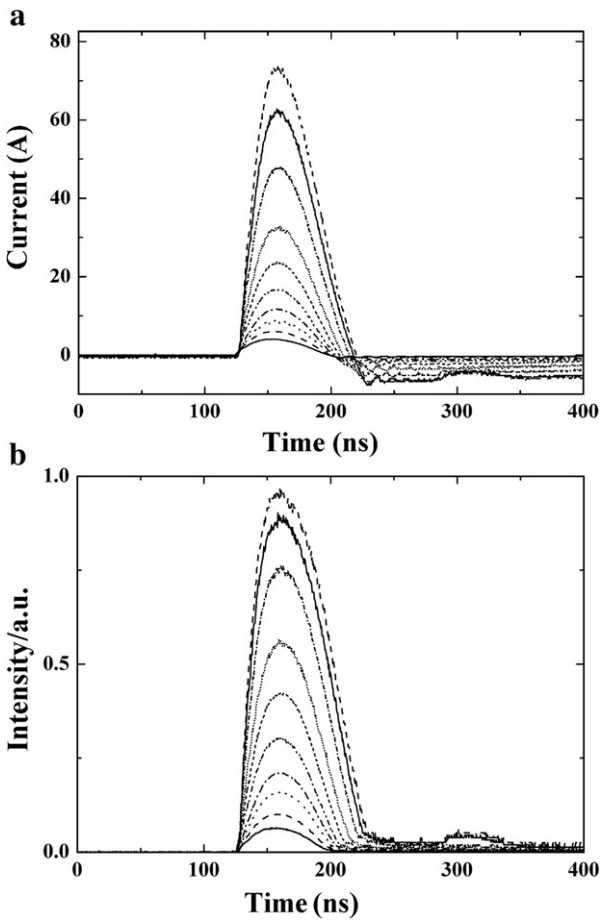

Fig. 9. (a) Linear array current pulse measurement. (b) Optical output pulse from the same electrical pulse.

frequency to drive the linear array. Such short pulsed operations with an infrequent repetition tend to inhibit the thermal rollover caused by joule heating. This can be proved by the wavelength shift under the nanosecond operation as indicated in Fig. 8. The wavelength shift rate is 0.026 nm/A, when the pulse operation current changes from 12 A to 80 A. However, the wavelength shift rate is 0.8 nm/A under CW operation due to the serious self-heating [18].

The linear array showed the ability to generate the narrow optical pulses. The optical pulse width tracks well with the electrical pulse width under short pulse excitation conditions. As can been seen from Fig. 9, the maximum optical pulse broadening factor is 1.25 and the amount of the broadening factor is likely the result of a complex interaction between the bias required to achieve the given current density, the VCSEL aperture size, diffusion capacitance, and the diode junction series resistance [19].

Fig. 10 shows the output power characteristics of the linear array under a short pulse current operation. As the heat generation of the

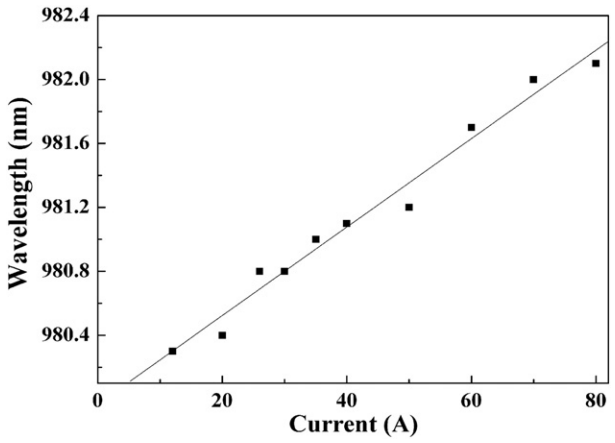

Fig. 8. Wavelength shift under pulse operation.

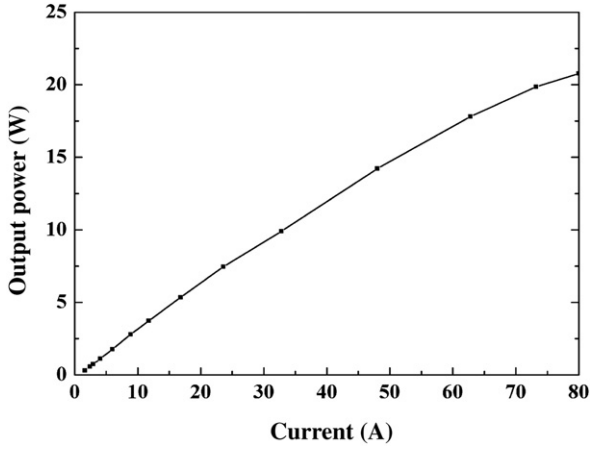

Fig. 10. The output power characteristic of the linear array under short pulse current.

linear array is suppressed due to the relatively short pulsed operation, a high output power can be expected. The linear array generates a peak pulse power of 20.8 W at an injection of 80 A with a repetition frequency of 1 kHz. A good balance among the output power, the far-field distribution, and the operation current is obtained through this configuration of a nonuniform array, which can provide high brightness and high efficiency for the applications of fiber coupling, solid laser pumping, and free-space communication. Higher optical power with a Gaussian beam profile could be expected with integrating more elements in such a nonuniform 2D configuration.

5. Conclusion

A nonuniform linear VCSEL array with a high power of 880 mW and a Gaussian far-field distribution is developed. As a comparison, a conventional 2D array exhibits a periodic intensity distribution at far field. The linear array also shows a better performance in the output power, lasing spectra, and far-field distribution. A peak power of over 20 W is achieved under a short pulsed operation with a repetition frequency of 1 kHz. Higher optical power with a Gaussian beam profile could be expected with integrating more elements in a nonuniform 2D configuration, which provides a good overall power efficiency for applications of high brightness and high coupling efficiency.

Acknowledgements

This work is supported by the National Science Foundations under contract numbers of 60636020, 60676034, 60706007, 10974012, 60876036, and 90923037, by the Jilin Province Science and Technology Development Project under the contract numbers of 20080335 and 20080516, and by the Chinese Academy of Sciences (CAS) Innovative Program.

References

[1] Weng W. Chow, Kent D. Choquette, Mary H. Crawford, Kevin L. Lear, G. Ronald Hadley, IEEE J. Quantum Electron. 33 (1997) 1810.
[2] I.G.A. Kenichi, Jpn. J. Appl. Phys. 47 (2008) 1.
[3] Markus C. Amann, Markus Ortsiefer, Robert Shau, Jurgen RoBkopf, Proc. SPIE 4871 (2002) 123.
[4] Elaine Wong, Xiaoxue Zhao, Connie J. Chang-Hasnain, Opt. commun. 281 (2008) 2218.
[5] Y.-C. Chang, C.S. Wang, L.A. Coldren, Electron. Lett. 43 (2007) 1022.
[6] Y.P. Lan, Yung-Fu Chen, K.F. Huang, H.C. Lai, J.S. Pan, IEEE Photon. Technol. Lett. 14 (2002) 272.
[7] Jian Wu, Gheorghe Iordache, Huw D. Sunners, John S. Roberts, Opt. commun. 196 (2001) 251.
[8] Vivien Verbrugge, Loig Plouzennec, Alain Le. Corre, Opt. commun. 214 (2002) 77.
[9] E. Kapon, C. Lindsey, J. Katz, S. Margalit, A. Yariv, Appl. Phys. Lett. 45 (1984) 200.
[10] E. Kapon, C.P. Lindsey, J.S. Smith, S. Margalit, A. Yariv, Appl. Phys. Lett. 45 (1984) 1257.
[11] N.K. Dutta, L.A. Koszi, B.P. Segner, S.G. Napholtz, Appl. Phys. Lett. 48 (1986) 312.
[12] Ping Li, Jianqiang Sun, Huimin Chen, Weirong Guo, Kun Li, Proc. SPIE 6824 (2007) 68241H.
[13] Martin Grabherr, Michael Miller, Roland Jager, Rainer Michalzik, Ulrich Martin, Heiko J. Unold, Karl Joachim Ebeling, IEEE J. Sel. Top. Quantum Electron. 5 (1999) 495.
[14] "Lasers and laser-related equipment. Test methods for laser beam parameters, beam widths, divergence angle and beam propagation factor," ISO 11146 (International Organization for Standardization, 1996).
[15] S.A. Riyopoulos, D. Dialetis, J. Liu, B. Riely, IEEE J. Sel. Top. Quantum Electron. 7 (2001) 312.
[16] Jean-Francois Seurin, Chuni L. Ghosh, Viktor Khalfin, Aleksandr Miglo, Guoyang Xu, James D. Wynn, Prachi Pradhan, L. Arthur D'Asaro, Proc. SPIE 6908 (2008) 690808.
[17] W. Nakwaski, M. Osinski, Electron Lett. 28 (1992) 572.
[18] Y. Sun, Z. Jin, Y. Ning, L. Qin, C. Yan, G. Luo, G. Tao, Y. Liu, L. Wang, D. Cui, H. Li, Z. Xu, Opt. Precision Eng. 12 (2004) 449.
[19] Jon Geske, Michael MacDougal, Garrett Cole, Donald Snyder, Proc. SPIE 6287 (2006) 628703.